data

MDPI

Article

Impact of Various Land Cover Transformations on Climate Change: Insights from a Spatial Panel Analysis

Mohsen Khezri

Department of Geography and Environment, London School of Economics and Political Science (LSE), London WC2A 2AE, UK; m.khezri@lse.ac.uk

Abstract: This study introduces an innovative empirical methodology by integrating spatial panel models with satellite imagery data from 1970 to 2019. This innovative approach illuminates the effects of greenhouse gas emissions, deforestation, and various global variables on regional temperature shifts and the environmental repercussions of land-use alterations, establishing a substantial empirical basis for climate change. The results revealed that global variables such as sunspot activity, the length of day (LOD), and the Global Mean Sea Level (GMSL) have negligible impacts on global temperature variations. This model uncovers the nuanced effect of deforestation on global temperatures, highlighting a decrease in temperature following deforestation above 40°N latitude, contrary to the warming effect observed in lower latitudes. Exceptionally, deforestation within the 10° N to 10° S tropical bands results in a temperature decrease, challenging the established theories. The results suggest that converting forests to grass/shrublands and croplands plays a significant role in these temperature dynamics.

Keywords: spatial panel models; climate change; deforestation; global climate models (GCMs); land cover

Academic Editor: Jamal Jokar Arsanjani

Received: 11 December 2024
Revised: 22 January 2025
Accepted: 28 January 2025
Published: 31 January 2025

Citation: Khezri, M. Impact of Various Land Cover Transformations on Climate Change: Insights from a Spatial Panel Analysis. *Data* **2025**, *10*, 19. https://doi.org/10.3390/data10020019

1. Introduction

Recent decades have witnessed profound transformations in forest landscapes, influenced by anthropogenic activities and natural events [1–4]. Against this backdrop, the adoption of measures for the protection, expansion, and improved management of forests globally stands out as one of the foremost natural strategies to curb global warming, aiming to keep temperature rises within a 1.5–2 degrees Celsius threshold; see Md Arif Hasan, 2021 [5,6]. This approach primarily leverages the cooling effects of afforestation, which includes carbon sequestration and some special biogeophysical processes, such as evaporative cooling, to mitigate climate change [7,8]. Consequently, forests are integral to carbon dioxide sequestration, with terrestrial ecosystems collectively mitigating 29% of annual CO_2 emissions [9]. This highlights the stark contrast in carbon storage capacity between deforested areas and their original forested conditions, with the former typically holding less carbon per unit area [10,11]. Nonetheless, beyond the implications for the carbon cycle, deforestation markedly influences local and regional climate patterns, altering a range of biogeophysical processes [12,13].

A theoretically complex balance of opposing effects governs the temperature dynamics of deforestation: warming due to increased atmospheric CO_2 and reduced latent heat flux and cooling attributed to higher albedo [14–17]. The biogeophysical impacts of deforestation on the climate are primarily manifested through the modifications to surface albedo, evapotranspiration (ET), and surface roughness length [18]. Forests influence the local

climate by absorbing more sunlight due to their low albedo, compared to brighter surfaces like bare soil, agricultural fields, or snow. This absorption can affect the global temperature by altering the radiation balance at the top of the Earth's atmosphere. Additionally, deep roots and a high leaf area make forests efficient at moving water from the land surface into the atmosphere via ET, producing latent heat. Thus, the sensible heat flux and associated surface temperature beneath the forest canopy are relatively low, especially during the growing season when ET is high [19–21]. The eradication of trees, which generally have deeper roots than crops and grasses, leads to a lower ET and, consequently, a decrease in the latent heat flux [11,22,23]. A decrease in canopy capture further facilitates this reduction in ET, reduced aerodynamic roughness length, and cooler temperatures post-deforestation, potentially affecting cloud formation and atmospheric properties [11,24–26]. These nonradiative processes stabilize the local climate by reducing both the diurnal temperature range and seasonal temperature extremes [13,27–29]. Therefore, these multifaceted impacts of deforestation present a significant challenge to the theoretical modeling of its effects on climate change.

Moreover, the underpinning theoretical assumptions have progressively evolved towards greater complexity. This is particularly evident in the context of forest biophysics' impact on climate, which exhibits substantial spatial variability. Nevertheless, this variability adheres to recognizable patterns discernible across different latitudes. A review of the extant literature reveals that the thermal dynamics associated with deforestation in high-latitude regions is primarily influenced by the albedo effect, resulting in a cooling impact on the climate. Specifically, while deforestation elevates the atmospheric CO_2 levels, the increase in albedo sufficiently offsets the warming from greenhouse gases, leading to a decrease in the surface air temperature (SAT) [11,21,30–32].

In contrast, in tropical regions, the abundant solar energy and moisture availability boost the processes of evapotranspiration (ET) and convection, inducing cooling effects throughout the year despite the regions' low albedo [33,34]. Therefore, deforestation at low latitudes results in a warmer climate. This temperature rise is mainly due to a decrease in ET and the prevailing effect of increased atmospheric CO_2, which overshadows the temperature signal [19,21,33,35,36]. However, the impact of deforestation at mid-latitudes is complex and remains uncertain, highlighted by the lower consensus among the models in this area [11,37,38]. Bala et al. [11] found that deforestation globally cools the climate because its effects on albedo and evapotranspiration outweigh the carbon-cycle warming. They also suggest that while tropical afforestation is beneficial, it could be counterproductive at high latitudes and only marginally helpful in temperate regions. According to Bonan's [1] study, tropical, temperate, and boreal reforestation and afforestation help reduce global warming by sequestering carbon, although additional factors significantly influence their net impact. For instance, the cooling effect of tropical forests is enhanced by the increased evaporation, while the low albedo of boreal forests can exert a warming influence. In contrast, the effect of temperate forests remains uncertain. Bonan emphasizes the need for interdisciplinary research to understand better these complex interactions and the full potential of forests in mitigating climate change, which is emphasized in this research.

The intricacies inherent in this domain have necessitated the development of various theory-based modeling approaches, each predicated on a distinct set of limiting assumptions. However, the outputs of these models may exhibit discrepancies when compared to empirical field measurements. For instance, recent research presents a conflicting view on the impact of deforestation on summer daytime temperatures, with satellite data showing increased temperatures in deforested areas [33,39,40], while some global climate models (GCMs), such as those from the Coupled Model Intercomparison Project Phase

5 (CMIP5) [41], the Land Use and Climate: Identification of Robust Impacts (LUCID) project [37,38], and the Community Earth System Model (CESM) [42], suggest a trend towards cooler daytime temperatures at the middle latitudes during summer, attributed to historical deforestation [43,44]. Moreover, emerging studies challenge the adequacy of these models by revealing unexpected climate dynamics, such as the Amazon rainforest now emitting more CO_2 than it absorbs even in slightly deforested areas [45], and the methane emissions from Amazonian tree stems vastly exceed those from temperate and tropical wetlands [46], as well as the substantial warming effects of non-CO_2 greenhouse gases neutralizing the cooling benefits of CO_2 absorption in the Amazon Basin [47]. These findings underscore the limitations of the current GCMs, rooted in both parameterization challenges and theoretical assumptions that fail to capture the complexity of climate systems.

Although various investigations accentuate the convoluted interconnections and adaptation mechanisms within global temperature series induced by anthropogenic and natural factors via econometric models [48–52], the econometric scrutiny of global warming determinants remains sparse, with spatial econometric models being notably underexploited. This study unveils an innovative empirical model that harnesses spatial panel models and satellite imagery from 1970 to 2019, aiming to bridge the divide between theoretical forecasts of climate impact and actual observational data. By offering fresh perspectives, this research pioneers in quantifying regional temperature variances by analyzing the influences of greenhouse gas emissions, deforestation, and various meteorological and global factors, including sunspot activity, the Earth's rotational duration, and the Global Mean Sea Level. Further, it delves into the environmental ramifications of deforestation across diverse latitudes and the climatic effects of transforming forested areas into non-forested land types, such as Cropland, Grass/shrubland, Pasture, and Sparse/no vegetation. This holistic methodology propels our comprehension of climate dynamics and substantially enriches the empirical underpinnings of environmental economics.

2. Methods

2.1. Empirical Model

In this research, we employ an extended version of spatial panel models to assess the influence of various determining factors on the temperature across different regions. Our analysis involves the estimation of diverse spatial models. Anselin et al. [53] outlined that a spatial panel model can incorporate a lagged dependent variable or adhere to a spatially autoregressive process within the error term. LeSage and Pace [54] have also introduced the spatial Durbin model, encompassing spatially lagged model-independent variables. Subsequently, we present the general formula for each of the three models. The formulations for the spatial lag model, spatial error model, and spatial Durbin model are as follows, respectively:

$$y_{it} = \varphi + x_{it}\beta + z_t\eta + \lambda\sum_{j=1}^{N} w_{ij}y_{jt} + c_i(optional) + \alpha_t(optional) + v_{it} \quad (1)$$

$$y_{it} = \varphi + x_{it}\beta + z_t\eta + c_i(optional) + \alpha_t(optional) + u_{it}, \quad u_{it} = \rho\sum_{j=1}^{N} w_{ij}u_{jt} + v_{it} \quad (2)$$

$$y_{it} = \varphi + x_{it}\beta + z_t\eta + \sum_{j=1}^{N} w_{ij}x_{jt}\theta + \lambda\sum_{j=1}^{N} w_{ij}y_{jt} + c_i(optional) + \alpha_t(optional) + v_{it} \quad (3)$$

In this context, y_{it} represents the dependent variable for a cross-sectional unit $i = 1, ..., N$ at time $t = 1, ..., T$. Meanwhile, x_{it} denotes a $1 \times K$ vector encompassing exogenous variables, and β is a $K \times 1$ vector representing the associated parameters. w_{ij} represents the element at the i-th row and j-th column in a pre-defined non-negative

$N \times N$ spatial weights matrix, denoted as w. The spatial Durbin model in Equation (3) extends the spatial lag model with independent variables of spatial lagging where θ is a $K \times 1$ vector of parameters. This research uses spatial econometric models to investigate the effects of temperature change determinants. The subsequent diagnostic tests confirm the selection of the spatial Durbin model specified in Equation (3) as the optimal choice. In spatial panel modeling, the Durbin model represents a comprehensive framework that subsumes both the spatial lag and spatial error models as specific cases. By incorporating spatially lagged dependent and independent variables, the Durbin model facilitates the examination of direct, indirect, and total spatial effects, thereby offering a nuanced approach to capturing the spatial dependencies. Additionally, the model accounts for spatial autocorrelation in the error structure, addressing the unobserved heterogeneity across spatial units. Consequently, this section introduces the experimental model, presented in the spatial Durbin form as Equation (4), facilitating a comprehensive understanding of the estimated model's structure.

$$\begin{aligned} lnTEM_{it} \;=\; & \beta_1 + \beta_2 DEF_{it} + \beta_3 lnGG_{it} + \beta_4 lnPRE_{it} + \beta_5 lnWINU_{it} + \beta_6 lnWINV_{it} + \beta_7 lnHCL_{it} + \beta_8 lnMCL_t + \\ & \beta_9 lnSUN_{it} + \beta_{10} lnLOD_{it} + \beta_{11} lnGMSL_{it} + \beta_{12} \textstyle\sum_{j=1}^{N} w_{ij} \times DEF_{it} + \beta_{13} \sum_{j=1}^{N} w_{ij} \times lnGG_{it} + \\ & \beta_{14} \textstyle\sum_{j=1}^{N} w_{ij} \times lnPRE_{it} + \beta_{15} \sum_{j=1}^{N} w_{ij} \times lnWINU_{it} + \beta_{16} \sum_{j=1}^{N} w_{ij} \times lnWINV_{it} + \beta_{17} \sum_{j=1}^{N} w_{ij} \times lnHCL_{it} + \\ & \beta_{18} \textstyle\sum_{j=1}^{N} w_{ij} \times lnMCL_{it} + \beta_{19} \sum_{j=1}^{N} w_{ij} \times lnTEM_{jt} + c_i(optional) + \alpha_t(optional) + v_{it} \end{aligned} \tag{4}$$

The spatial Durbin model comprises three variable categories. The initial category encompasses domestic exogenous variables within regions. In this study, the logarithm of the temperature ($lnTEM$) is considered as a function of deforestation (DEF), the logarithm of greenhouse gas emissions ($lnGG$), mean sea level pressure ($lnPRE$), 100 m u-component ($lnWINU$), 100 m v-component of wind ($lnWINV$), high cloud cover ($lnHCL$), and Medium and Low cloud cover ($lnMCL$), as domestic exogenous variables within regions. The variables in the second category pertain to global factors, where the temperature of regions is modeled as a function of the logarithm of total sunspot number ($lnSUN$), length of day ($lnLOD$), and Global Mean Sea Level ($lnGMSL$). Moreover, the third category comprises spatial variables, which represent the weighted average of internal variables from neighboring regions, denoted as $\sum_{j=1}^{N} w_{ij} \times x_{jt}$ in Equation (4). These third-category variables investigate how the environmental conditions in neighboring regions impact the temperature conditions of the specific country. The methodology for variable selection in this research is straightforward. We attribute climate change to either anthropogenic factors (including DEF and $lnGG$) or natural variations in climatic parameters (including $lnPRE$, $lnWINU$, $lnWINV$, $lnHCL$, $lnMCL$), alongside shifts in global dynamics (including $lnLOD$, $lnGMSL$, $lnSUN$). While the impact of human activities is well documented, we also consider the potential influence of other climatic and global factors. However, our analysis reveals that the model's outcomes are largely unaffected by the variations in these climatic parameters, underscoring human activities as the primary driver of global warming over the past five decades—a focal point of thorough investigation in this study.

While the model could be enhanced by incorporating additional variables, we have selected three critical global variables in alignment with the established literature. Earth Orientation Parameters (EOPs) constitute a set of parameters that elucidate the irregularities in the Earth's rotation [55]. The length of day (LOD) is a critical factor in modeling the Earth's rotation rate fluctuations, which change due to gravitational influences from external celestial bodies and geophysical processes within various Earth layers. Significant events such as El Niño have manifested through observable signals in the length of day (LOD) data [56]. According to Zotov et al. [57], analogous quasi-periodic oscillations of approximately 60 and 20 years have been identified in the global mean Earth temperature anomaly (HadCRUT4) and Global Mean Sea Level (GMSL). Comparable cycles have also

been observed in the LOD to indicate Earth rotation variations. As a result, they posit a connection between the Earth's rotation and climate indices. Ding et al. [58] substantiate the correlation between the approximately 64-year oscillation in sea level changes and fluctuations in the Earth's magnetic field dipole, as well as the approximately 65-year oscillation in ΔLOD. Research in this domain typically presents the findings on the impact of variable changes, such as the LOD, on climate change in an inconclusive manner. This ambiguity arises from the intricate and multi-dimensional nature of the factors influencing climate change, making it challenging to accurately assess the effects of local variables due to dominant factors. A global model is essential to achieve a comprehensive understanding of climate change.

2.2. Data

Addressing the prominent challenge in climate change time series analysis—limited data accessibility—we undertook an innovative approach to generate the requisite data for our research, collecting data spanning from 1970 to 2019. The variables, including their sources and structural details, are outlined in Table 1 before their incorporation into the analysis. We restricted our analysis to data from regions between a latitude of 60 degrees south and 80 degrees north. Moreover, we included only those areas where water constitute less than 10% of the total area. To refine our analysis further, we assembled panel data for 232 regions, spanning 1970 through 2019. We have differentiated between the 100 m u-component ($lnWINU$) and 100 m v-component of wind ($lnWINV$) across the northern and southern hemispheres, considering the four cardinal directions, to account for potential asymmetries. The specifics of this categorization are detailed in Table 1.

Table 1. Variables constructed.

Variable	Variable Constructed	Source
$lnTEM$	$= log(Tem_{it})$; Tem_{it} = temperature in the region i in period t	NASA
DEF	=deforestation calculated by the land use/cover states and transition layers	Winkler et al. [59]
$lnGG$	$= log(1 + 10^{22} \times GG_{it})$; CO_{2it} = Global Greenhouse Gas Emissions.	Crippa et al. [60]
$lnPRE$	$= log(1 + PRE_{it})$; PRE_{it} = Mean sea level pressure	Hersbach et al. [61]
$lnWINUn+$	$= log(1 + 10^3 \times WINUn+_{it})$; $WINUn+_{it}$ = 100 m u-component of wind from the west in the northern hemisphere	Hersbach et al. [61]
$lnWINUn-$	$= log(1 + 10^3 \times WINUn-_{it})$; $WINUn_{it}$ = 100 m u-component of wind from the east in the northern hemisphere	Hersbach et al. [61]
$lnWINVn+$	$= log(1 + 10^3 \times WINVn+_{it})$; $WINVn+_{it}$ = 100 m v-component of wind from the south in the northern hemisphere	Hersbach et al. [61]
$lnWINVn-$	$= log(1 + 10^3 \times WINVn-_{it})$; $WINVn-_{it}$ = 100 m v-component of wind from the north in the northern hemisphere	Hersbach et al. [61]
$lnWINUs+$	$= log(1 + 10^3 \times WINUs+_{it})$; $WINUs+_{it}$ = 100 m u-component of wind from the west in the southern hemisphere	Hersbach et al. [61]
$lnWINUs-$	$= log(1 + 10^3 \times WINUs-_{it})$; $WINUs_{it}$ = 100 m u-component of wind from the east in the southern hemisphere	Hersbach et al. [61]
$lnWINVs+$	$= log(1 + 10^3 \times WINVs+_{it})$; $WINVs+_{it}$ = 100 m v-component of wind from the south in the southern hemisphere	Hersbach et al. [61]
$lnWINVs-$	$= log(1 + 10^3 \times WINVs-_{it})$; $WINVs-_{it}$ = 100 m v-component of wind from the north in the southern hemisphere	Hersbach et al. [61]

Table 1. *Cont.*

Variable	Variable Constructed	Source
$lnHCL$	$= log(1 + 10^8 \times HCL_{it})$; HCL_{it} = High cloud cover	Hersbach et al. [61]
$lnMCL$	$= log(1 + 10^8 \times HCL_{it})$; MCL_{it} = Medium and Low cloud cover	Hersbach et al. [61]
$lnSunspot$	$= log(Sun_{it})$ Sun_{it} = total sunspot number	SILSO
$lnLOD$	$= log(10^3 \times LOD_{it} + 0.2)$ LOD_{it} = length of day (LOD)	IERS
$lnGMSL$	$= log(GMSL_{it} + 85)$ $GMSL_{it}$ = Global Mean Sea Level	Frederikse et al. [62] and Beckley et al. [63]

NASA: National Aeronautics and Space Administration; https://data.giss.nasa.gov/gistemp/ (accessed on 21 January 2024). SILSO: Solar Influences Data Analysis Center; https://www.sidc.be/SILSO/datafiles (accessed on 21 January 2024). IERS: International Earth Rotation and Reference Systems Service; https://www.iers.org/IERS/EN/DataProducts/EarthOrientationData/eop.html (accessed on 21 January 2024).

2.3. Spatial Dependence on the Temperature of World Regions

Employing satellite maps delineated in Table 1, we harnessed diverse variables with varying grid structures and temporal scopes. The regional correlation in temperature change is shown in Figure 1, giving rise to two essential questions that must be addressed for confirmation: 1. Has the temperature genuinely experienced regional fluctuations? 2. What is the extent of this regional area? To address these questions, we employed the non-parametric spatial correlogram method [64] shown in Figure 2. This figure indicates that regions within a proximity of approximately 2000 km have undergone concurrent temperature fluctuations. In contrast, those within this range either exhibited no mutual influence or demonstrated adverse impacts on each other.

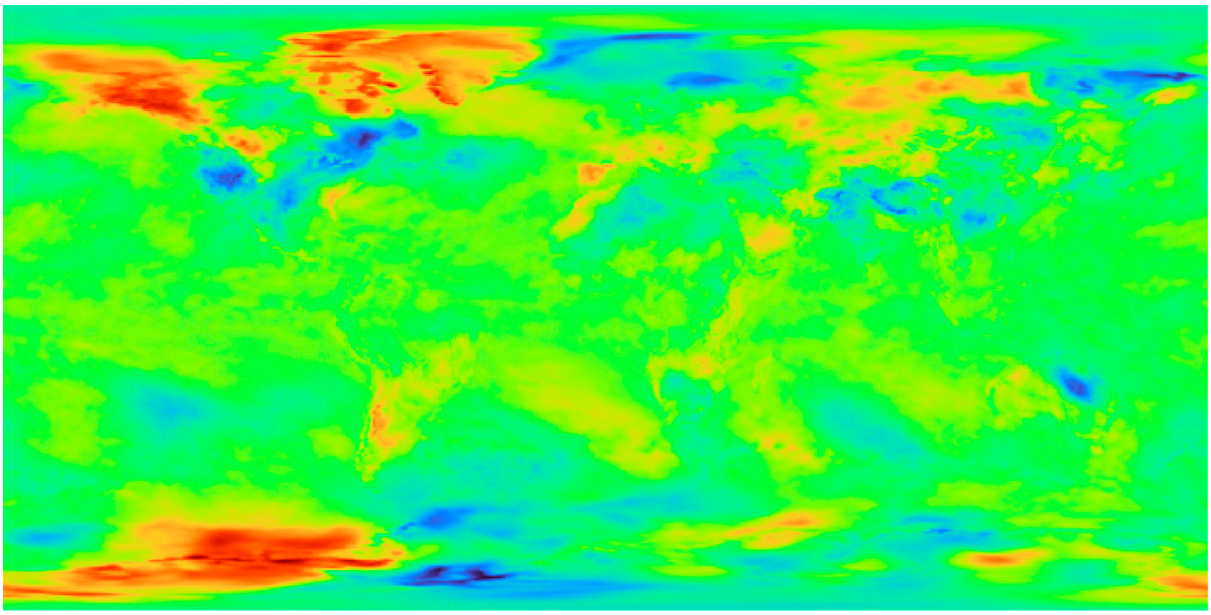

Figure 1. *Cont.*

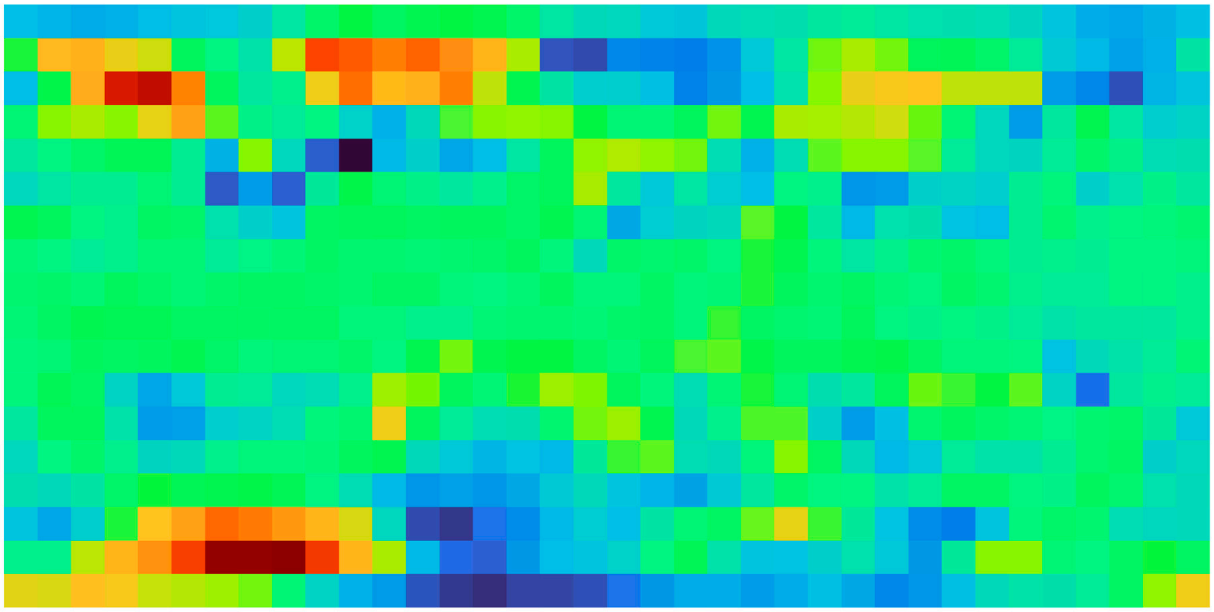

Figure 1. The variations in temperature among the regions under investigation during the year 2019. As the color spectrum changes from blue to red, the temperature of the area increases. The above figure depicts temperature changes in 2019 using a standardized $2^\circ \times 2^\circ$ grid, where each grid cell spans 2 degrees of latitude by 2 degrees of longitude. To ensure uniformity across all maps, mitigate outlier influences, and streamline computational processes, we homogenized all variables onto a consistent $1000^\circ \times 1000^\circ$ grid. The bottom figure exemplifies this transformation, showcasing the computation of averaged temperature changes within the region of interest. This methodological approach extends to our treatment of other maps in the study.

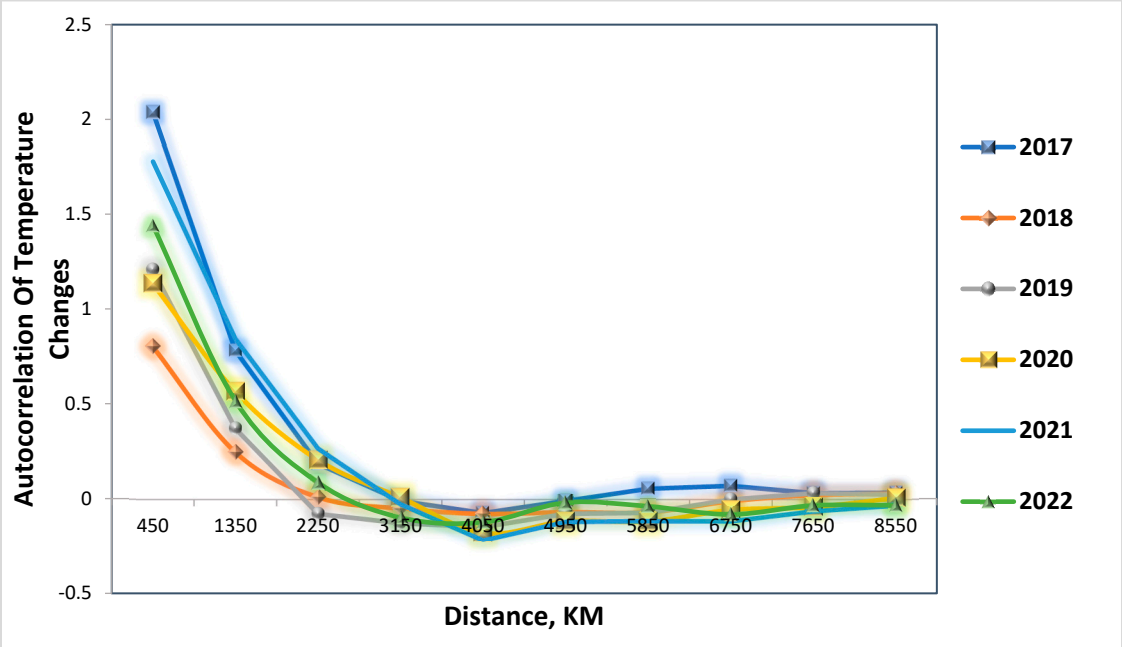

Figure 2. The non-parametric spatial correlogram for evaluating global spatial autocorrelation with distance. This figure visually represents how spatial autocorrelation changes with distance using the non-parametric spatial correlogram for 2017 to 2023. Beyond a certain range of about 2000 km to 3000 km, the autocorrelation initially becomes negative and subsequently fluctuates around the zero line.

We applied the outlined procedure to various meteorological variables, yielding comparable results. However, one of the pivotal influencers on temperature fluctuations is

alterations in the land conditions, manifesting as deforestation, shifts in land utilization, and related factors. Our computations for the targeted variables were grounded in data from Winkler et al. [59], organized in a $1^\circ \times 1^\circ$ grid. This dataset not only encapsulates the evolution of land cover over different years but also delineates the shifts between distinct plant covers, namely (1) Urban, (2) Cropland, (3) Pasture, (4) Forest (Unknown/Other), (5) Forest (Evergreen, needle leaf), (6) Forest (Evergreen, broad leaf), (7) Forest (Deciduous, needle leaf), (8) Forest (Deciduous, broad leaf), (9) Forest (Mixed), (10) Grass/shrubland, and (11) Sparse/no vegetation. The global vegetation cover in 2019 is depicted in Figure 3; our focus, however, lies in elucidating how a specific vegetation type in a given year transforms into a different kind in the subsequent year. We accomplished this analysis utilizing the transfer data available in the database, where 11 vegetation types can transition in 121 possible ways. Over the past five decades, most of these transitions occurred from Pasture to Forest (Deciduous, broad leaf). To illustrate, we present the case of this specific transition, employing the MATLAB programming language in Figure 3.

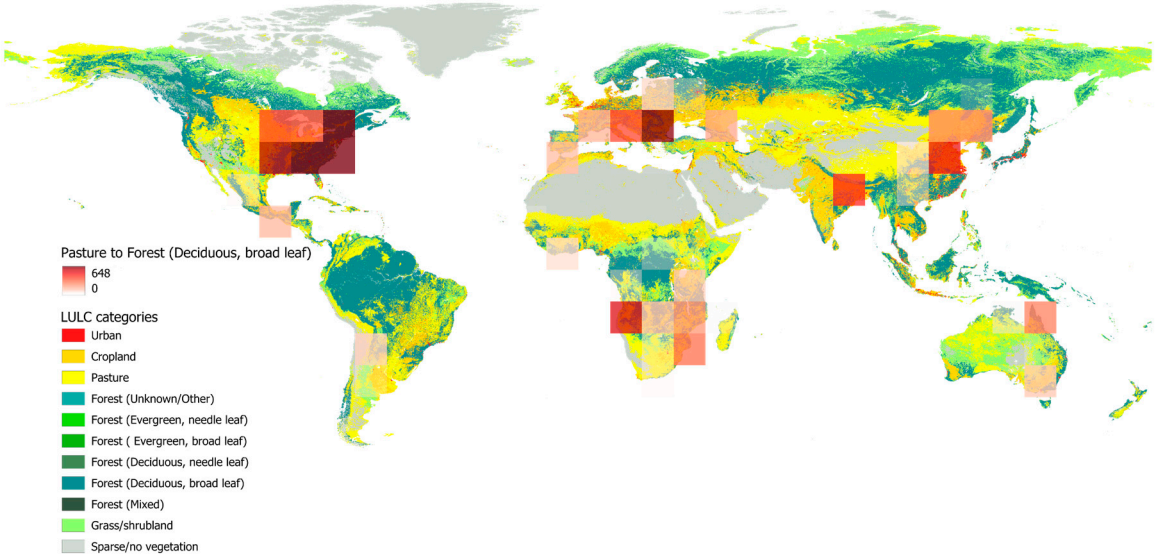

Figure 3. Global map for land cover. The illustration consists of two components. The initial segment comprises regions featuring $1000^\circ \times 1000^\circ$ grids, depicting the transition from Pasture to Deciduous, broadleaf forest. The second segment displays the Earth's vegetation cover in the year 2019. By considering a grid with dimensions of $1000^\circ \times 1000^\circ$, we quantified the occurrences of the transition from Pasture to Forest (Deciduous, broad leaf) in $1^\circ \times 1^\circ$ grids. The corresponding count graph is highlighted in red. Notably, regions with a deeper shade of red indicate a higher frequency of the mentioned transition. By employing this method, we can ascertain the extent of transfers in an area of approximately 1110 by 1110 square kilometers. These calculations were systematically applied across all 121 possible states of land cover changes.

After evaluating transfers across 121 states, we computed the net transfer rates for each state. For instance, the net transfer from Forest (Deciduous, broad leaf) to Pasture is determined by subtracting the transfer from Forest (Deciduous, broad leaf) to Pasture from the transfer from Pasture to Forest (Deciduous, broad leaf) in a specific year and region. Positive transfer values signify an overall transition from Forest (Deciduous, broad leaf) to Pasture, whereas negative values indicate the opposite. The analyzed data present the variations in forest coverage across different years. To obtain a comprehensive view of the trends in forest changes over these years, we performed cumulative calculations of these changes annually, aiming to discern the trend patterns in the variations within the vegetation cover across different regions.

This study's primary focus revolves around transforming forest vegetation into alternative non-forest vegetation, as illustrated in Figure 4. This figure highlights an overall negative transformation in vegetation cover within forests classified as unknown/other. This signifies a substantial conversion of Pasture and Cropland into this particular type of forest, showing that human planting activities, potentially involving orchards, predominantly contribute to this forest type. A comparable examination can be extended to other land categories, as demonstrated in Figure 4. Additionally, the Deciduous and needle-leaf Forest category predominantly expands by transitioning from Grassland/Shrubland into forested areas. Conversely, for other forest categories, the data exhibit positive transitions that signify a net increase in deforestation.

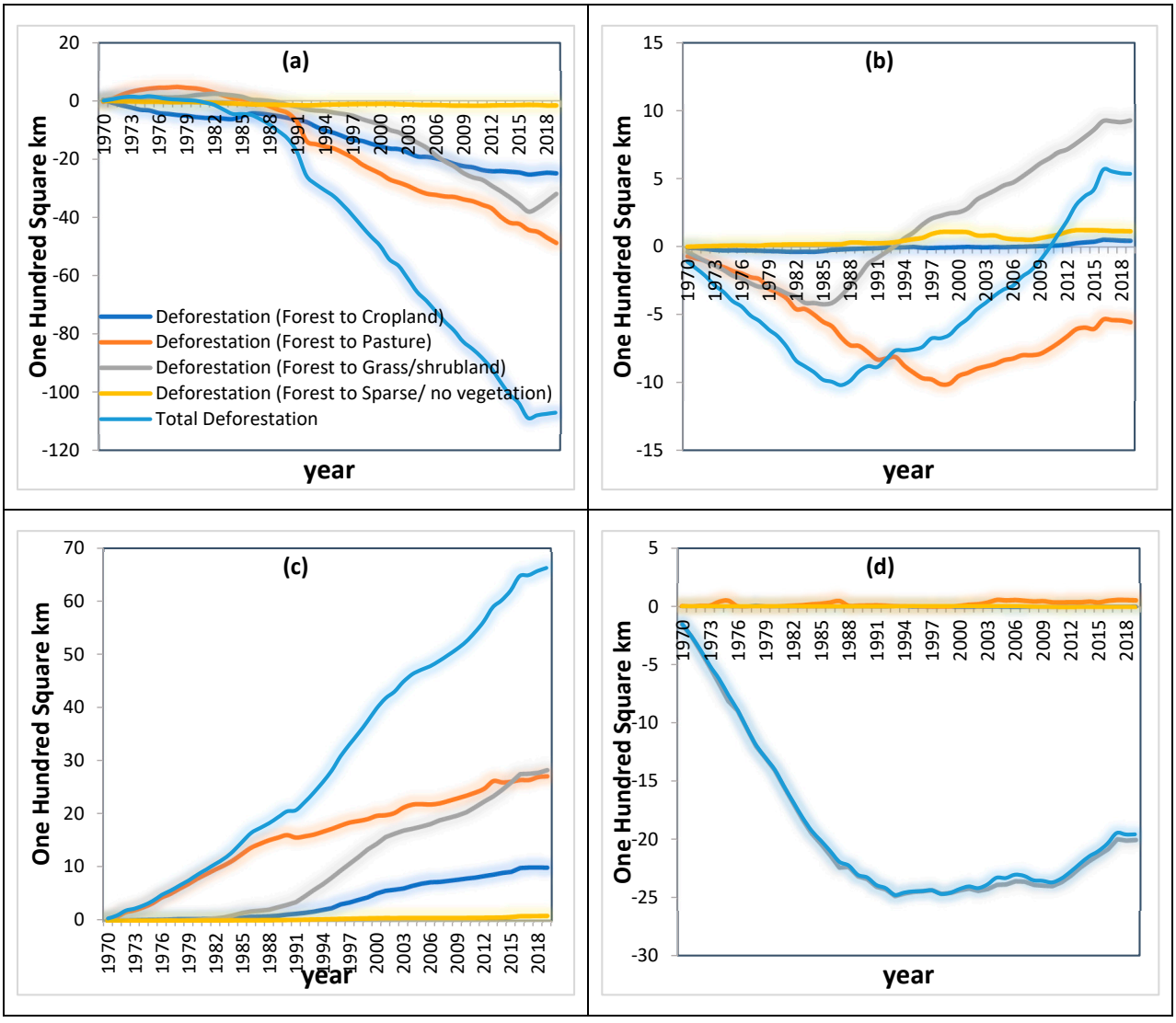

Figure 4. *Cont.*

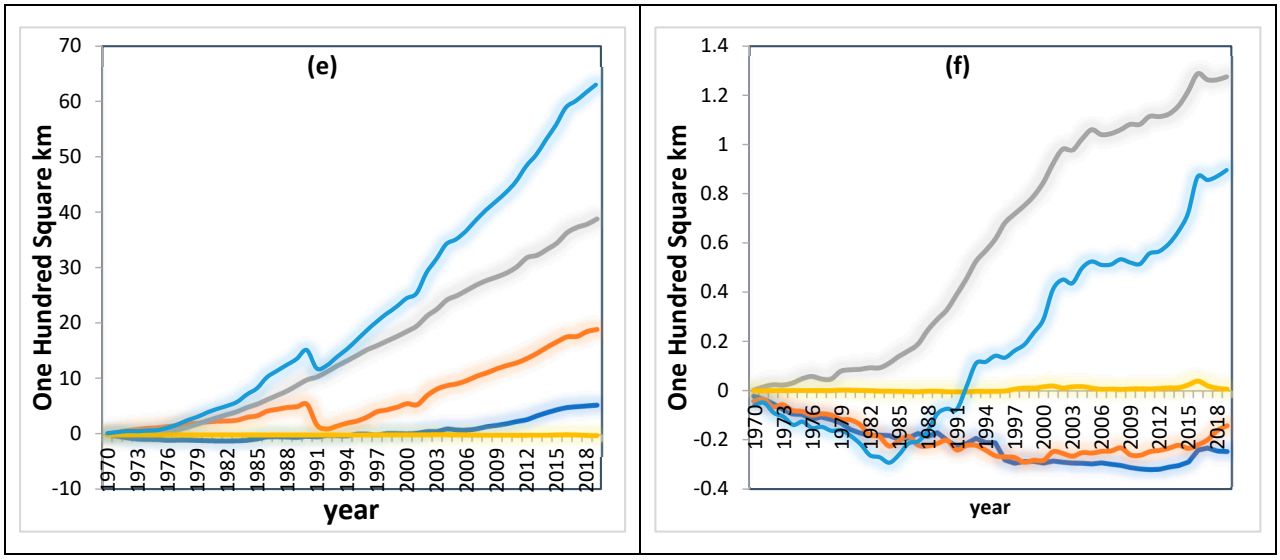

Figure 4. (**a**) **Transformation from Forest (Unknown/Other) to Alternative Non-Forest Vegetation.** (**b**) **Transformation from Forest (Evergreen, needle leaf).** (**c**) **Transformation from Forest (Evergreen, broad leaf).** (**d**) **Transformation from Forest (Deciduous, needle leaf).** (**e**) **Transformation from Forest (Deciduous, broad leaf).** (**f**) **Transformation from Forest (Mixed).** The provided values represent cumulative transfer in forest cover. Consequently, using 1970 as the reference year, the figures for 2019 reflect the aggregate deforestation that had transpired up to that year relative to 1970.

3. Results

3.1. Optimal Weight Matrix

In this section, our initial focus is on identifying the most effective model and optimal weight matrix. Figure 5 showcases the outcomes of estimating Model 1 in Tables 2 and 3 across various regional domains using distinct weight matrices. The air temperature's vertical axis is on the right side, while the vertical axes for the other two variables are on the left. Our exploration spans weight matrices from 2000 km to 14,000 km. These estimations aim to scrutinize result sensitivity, pinpointing the regional radius where the model exhibits optimal performance. As illustrated in Figure 5, this variable's most optimal weight matrix is observed within a 14,000 km radius for greenhouse gas emissions and 8000 km for deforestation. Intriguingly, our analysis identifies a significant peak in deforestation at approximately 2500 km, which likely reflects the albedo effect due to its radiative and thermal interactions with adjacent areas. As the scale of observation expands, the impacts of greenhouse gases progressively manifest globally, underscoring the interconnectedness of local environmental changes and global climatic dynamics.

Table 2. Diagnostic tests for optimal model selection.

Hausman test — statistic	561.5	538.6	714.0	453.1	529.6
	(0.000)	(0.000)	(0.000)	(0.000)	(0.000)
LM spatial lag	4902.4	5698.6	6416.3	6832.1	7564.4
	(0.000)	(0.000)	(0.000)	(0.000)	(0.000)
LM spatial error	420.3	573.7	589.4	679.8	653.3
	(0.000)	(0.000)	(0.000)	(0.000)	(0.000)
Wald test for the spatial Durbin model against the spatial lag model	1040.0	1026.7	1035.1	1021.8	1015.0
	(0.000)	(0.000)	(0.000)	(0.000)	(0.000)
Wald test for the spatial Durbin model against the spatial error model	527.3	467.5	526.6	473.2	466.6
	(0.000)	(0.000)	(0.000)	(0.000)	(0.000)
LR test for the spatial Durbin model against the spatial lag model	1019.3	1004.3	1015.1	1001.6	993.1
	(0.000)	(0.000)	(0.000)	(0.000)	(0.000)
LR test for the spatial Durbin model against the spatial error model	530.0	466.2	516.9	479.5	472.2
	(0.000)	(0.000)	(0.000)	(0.000)	(0.000)

Table 3. The results of estimating Equation (4).

	Model 1	**Model 2**	**Model 3**	**Model 4**	**Model 5**
Total Deforestation	0.00004 (0.013)	0.00005 (0.002)	0.00004 (0.013)	0.00004 (0.013)	0.00004 (0.013)
lnGG	0.00012 (0.153)		0.00011 (0.156)	0.00011 (0.157)	0.00013 (0.120)
lnPRE	−0.84616 (0.000)	−0.84716 (0.000)	−0.84656 (0.000)	−0.84612 (0.000)	−0.84621 (0.000)
lnWINUn +	0.00010 (0.000)	0.00010 (0.000)	0.00010 (0.000)	0.00010 (0.000)	0.00010 (0.000)
lnWINUn −	0.00009 (0.000)	0.00009 (0.000)	0.00009 (0.000)	0.00009 (0.000)	0.00009 (0.000)
lnWINVn +	0.00010 (0.000)	0.00010 (0.000)	0.00010 (0.000)	0.00010 (0.000)	0.00010 (0.000)
lnWINVn −	−0.00003 (0.201)	−0.00003 (0.180)	−0.00003 (0.200)	−0.00003 (0.202)	−0.00003 (0.200)
lnWINUs +	−0.00004 (0.466)	−0.00004 (0.538)	−0.00004 (0.469)	−0.00004 (0.470)	−0.00004 (0.466)
lnWINUs −	−0.00005 (0.364)	−0.00004 (0.482)	−0.00005 (0.369)	−0.00005 (0.367)	−0.00005 (0.365)
lnWINVs +	−0.00008 (0.078)	−0.00007 (0.097)	−0.00008 (0.077)	−0.00008 (0.078)	−0.00007 (0.083)
lnWINVs −	0.00002 (0.646)	0.00002 (0.573)	0.00002 (0.650)	0.00002 (0.644)	0.00002 (0.627)
lnHCL	0.00174 (0.000)	0.00174 (0.000)	0.00174 (0.000)	0.00174 (0.000)	0.00174 (0.000)
lnMCL	−0.00155 (0.000)	−0.00154 (0.000)	−0.00155 (0.000)	−0.00155 (0.000)	−0.00155 (0.000)
lnSunspot			−0.00001 (0.427)		
lnLOD				0.00002 (0.706)	
lnGMSL					0.00003 (0.168)
$W \times$ *Total Deforestation*	−0.00039 (0.000)	−0.00039 (0.000)	−0.00040 (0.000)	−0.00039 (0.000)	−0.00038 (0.000)
$W \times lnCO2$	0.00058 (0.000)		0.00059 (0.000)	0.00060 (0.000)	0.00040 (0.017)
$W \times lnPRE$	0.86778 (0.000)	0.87371 (0.000)	0.86709 (0.000)	0.86829 (0.000)	0.86833 (0.000)
$W \times lnWINUn +$	0.00012 (0.008)	0.00011 (0.009)	0.00012 (0.009)	0.00012 (0.009)	0.00012 (0.008)
$W \times lnWINUn -$	0.00010 (0.033)	0.00009 (0.034)	0.00009 (0.035)	0.00009 (0.033)	0.00010 (0.032)
$W \times lnWINVn +$	0.00003 (0.481)	0.00002 (0.642)	0.00003 (0.467)	0.00003 (0.484)	0.00003 (0.491)
$W \times lnWINVn -$	−0.00007 (0.068)	−0.00008 (0.042)	−0.00007 (0.066)	−0.00007 (0.070)	−0.00007 (0.068)
$W \times lnWINUs +$	−0.00003 (0.733)	−0.00001 (0.873)	−0.00003 (0.743)	−0.00003 (0.742)	−0.00003 (0.728)
$W \times lnWINUs -$	0.00010 (0.245)	0.00014 (0.114)	0.00010 (0.235)	0.00010 (0.239)	0.00010 (0.243)
$W \times lnWINVs +$	−0.00001 (0.842)	0.00001 (0.874)	−0.00001 (0.836)	−0.00001 (0.850)	−0.00001 (0.876)
$W \times lnWINVs -$	−0.00006 (0.370)	−0.00003 (0.592)	−0.00006 (0.374)	−0.00006 (0.372)	−0.00005 (0.388)
$W \times lnHCL$	−0.00030 (0.119)	−0.00026 (0.166)	−0.00028 (0.139)	−0.00030 (0.110)	−0.00030 (0.111)
$W \times lnMCL$	−0.00041 (0.064)	−0.00048 (0.031)	−0.00044 (0.048)	−0.00040 (0.070)	−0.00041 (0.066)
$W \times lnTem$	0.86097 (0.000)	0.86997 (0.000)	0.85699 (0.000)	0.86296 (0.000)	0.86297 (0.000)
R^2	0.9987	0.9987	0.9987	0.9987	0.9987
$log - likelihood$	54,956.8	54,919.7	54,956.2	54,956.9	54,957.9

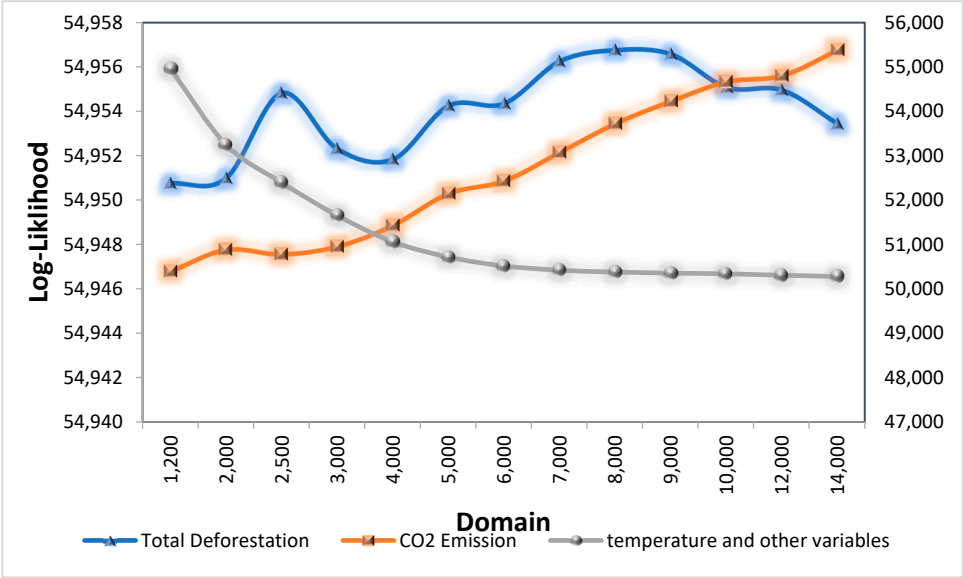

Figure 5. The sensitivity of the estimation results for weight matrices in different regional domains. Initially, we examined the model's sensitivity to modifications in the weight matrix associated with the air temperature variable. Consistent with our prior tests, this variable demonstrated maximum log-likelihood within a 2000 km radius. Subsequently, we amplified the weights matrix for greenhouse gas emissions to maintain the territory's stability covered by the variable size weights matrix at the 2000 km level. As illustrated in Figure 5, the most optimal weight matrix for this variable is observed within a 14,000 km radius, highlighting the global impact of this variable on temperature adjustments across regions. Following this, we expanded the territory covered by the deforestation weight matrix while holding the radius of greenhouse gas emissions constant at 14,000 km. The outcomes revealed that the effects of this variable manifest within an 8000 km radius, underscoring the global dimensions of its influence.

3.2. Diagnostic Tests

First, we aimed to identify the most appropriate model specification by employing a range of diagnostic tests. As part of this process, we performed a series of Lagrange Multiplier (LM) tests, summarized in Table 2, to assess the impact of incorporating spatial lag and spatial error terms into the models. These tests were designed to detect potential spatial dependence or autocorrelation that may otherwise remain unaccounted for. The results in Table 2 show that all the test statistics are significant at the one percent level across all the models. This strong evidence underscores the critical need to include both spatial lagged and spatial error effects to achieve a more comprehensive and accurate model fit. The alternative hypothesis in the LR or Wald test confirms the presence of the spatial lagged independent variable in the model. Statistically significant LR or Wald test results were observed across all the models, concluding that the spatial Durbin model with the spatial lagged independent variable was ultimately chosen for the estimation analyses. Furthermore, Table 2 incorporates the outcomes from the Hausman test, confirming the presence of fixed effects at a significance level of 1%.

We initially endeavored to examine the impact of global variables on temperature fluctuations. To achieve this, Table 3 displays the estimates from five distinct models. Model 1 encompasses all variables, while in Model 2, greenhouse gas emissions are omitted to explore their potential co-linearity with deforestation. Furthermore, in the subsequent models (3 to 5), the individual presentation of global variables is undertaken to assess potential collinearity.

Moreover, the inclusion of spatial fixed effects significantly enhanced the model's explanatory power, as evidenced by a higher R^2 value. This improvement occurred because

of the geographical locations for the majority of the climate variability and temperature differences across regions within a given year. Consequently, identification tests confirmed that incorporating fixed effects is essential for accurate modeling.

3.3. Results of the Estimations

Initially, estimating Equation (4), as delineated in the appendix, is imperative. Nevertheless, this equation alone cannot constitute the basis for the result analysis. The inclusion of the variable $W \times lnTem$ complicates the interpretation by reintroducing the temperatures of adjacent regions into the model, thereby blending the effects of variables pertinent to both the focal region and its surrounding areas via the temperature variable of neighboring regions. This integration of variables affects their marginal impacts. Thus, by utilizing the estimated results derived from Equation (4), our objective is to meticulously assess both the direct and indirect marginal effects of variables on temperature variations. Direct effects gauge the influence of an independent variable on the dependent variable within a spatially connected region. Additionally, indirect effects measure a specific region's independent variables' impact on the neighboring regions' dependent variable. Table 4 delineates the independent variables' direct and indirect effects across diverse regional domains. To concisely summarize the outcomes, we have elected to omit the reporting of the coefficients of climate variables in models 2 through 5.

Table 4. The marginal effects of variables of the temperature.

	Model 1					
	Total Effects		**Direct Effects**		**Indirect Effects**	
$Total\ Deforestation$	−0.00248	(0.000)	−0.00015	(0.000)	−0.00233	(0.000)
$lnGG$	0.00503	(0.000)	0.00049	(0.000)	0.00454	(0.000)
$lnPRE$	0.15833	(0.051)	−0.77072	(0.000)	0.92905	(0.000)
$lnWINUn+$	0.00153	(0.000)	0.00021	(0.000)	0.00132	(0.000)
$lnWINUn-$	0.00134	(0.000)	0.00019	(0.000)	0.00116	(0.000)
$lnWINVn+$	0.00090	(0.003)	0.00016	(0.000)	0.00074	(0.008)
$lnWINVn-$	−0.00072	(0.018)	−0.00008	(0.024)	−0.00064	(0.020)
$lnWINUs+$	−0.00053	(0.455)	−0.00008	(0.380)	−0.00044	(0.479)
$lnWINUs-$	0.00036	(0.596)	−0.00002	(0.817)	0.00038	(0.530)
$lnWINVs+$	−0.00067	(0.178)	−0.00012	(0.068)	−0.00055	(0.215)
$lnWINVs-$	−0.00029	(0.545)	−0.00001	(0.919)	−0.00029	(0.506)
$lnHCL$	0.01030	(0.000)	0.00239	(0.000)	0.00791	(0.000)
$lnMCL$	−0.01408	(0.000)	−0.00251	(0.000)	−0.01157	(0.000)
	Model 2					
$Total\ Deforestation$	−0.00261	(0.000)	−0.00015	(0.000)	−0.00246	(0.000)
$lnPRE$	0.20798	(0.016)	−0.76724	(0.000)	0.97522	(0.000)
	Model 3					
$Total\ Deforestation$	−0.00249	(0.000)	−0.00016	(0.000)	−0.00233	(0.000)
$lnGG$	0.00492	(0.000)	0.00050	(0.000)	0.00442	(0.000)
$lnPRE$	0.14667	(0.056)	−0.76631	(0.000)	0.91298	(0.000)
$lnSunspot$	−0.00009	(0.427)	−0.00002	(0.426)	−0.00007	(0.427)
	Model 4					
$Total\ Deforestation$	−0.00253	(0.000)	−0.00016	(0.000)	−0.00237	(0.000)
$lnGG$	0.00524	(0.000)	0.00051	(0.000)	0.00473	(0.000)
$lnLOD$	0.00014	(0.707)	0.00003	(0.707)	0.00011	(0.707)
	Model 5					
$Total\ Deforestation$	−0.00245	(0.000)	−0.00015	(0.000)	−0.00229	(0.000)
$lnGG$	0.00383	(0.000)	0.00042	(0.000)	0.00341	(0.000)
$lnPRE$	0.16355	(0.046)	−0.76645	(0.000)	0.93001	(0.000)
$lnGMSL$	0.00026	(0.156)	0.00005	(0.155)	0.00020	(0.156)

Based on the estimation results of Table 4, the logarithm of sunspots, length of day (LOD), and Global Mean Sea Level (GMSL) demonstrate insignificant effects, leading to their exclusion from the model due to its inability to significantly contribute to explaining the temperature differences among regions. We conducted a thorough examination but found no instances where the identified variables could account for the variations in weather patterns. We also explored the potential co-linearity with meteorological variables, yet no significant effects emerged.

Consequently, the estimations reveal that temperature fluctuations are affected by various variables in the model, with greenhouse gas emissions being the primary driver. A one percent increase in emissions leads to a 0.005% rise in regional temperatures, with an indirect effect accounting for 0.0045% of this change. Additionally, a rise in mean sea level pressure reduces local temperatures by 0.77% while increasing neighboring regions' temperatures by about 0.929%, resulting in a net effect of roughly 0.158%. The findings also indicate significant influences from the wind in the northern hemisphere: the u-wind's east and west components contribute to temperature increases, whereas the v-wind component lowers the air temperature when originating from the north and polar regions, with a southward wind causing a rise. Lastly, high cloud cover warms the air, while low and medium cloud cover have a cooling effect.

Moreover, deforestation is the critical factor in this study, and it has yielded results contrary to our initial theoretical expectations. The rise in deforestation has resulted in a reduction in temperature. Furthermore, these effects have manifested predominantly on a regional scale. To delve deeper into the reasons behind these outcomes, we have persistently assessed various aspects of forest changes.

To enhance our analysis, we investigated the impacts of total deforestation across various geographical latitudes. Considering that the geographic latitudes span from 50 degrees south to 80 degrees north as the foundation for our estimates, we segmented this range into 10-degree intervals and investigated the impacts of deforestation on temperature across latitudes, as detailed in Table 5. By analyzing the impact of deforestation within each interval across various models, we derived approximately 14 distinct models. The estimation outputs resemble those detailed in Tables 3 and 4 for each model. Given the extensive computational effort involved, we opted to withhold the detailed results report for all latitudes, summarizing only the most pertinent findings concerning the marginal effects of deforestation at each segment in Table 5.

Table 5. The marginal effects of total deforestation across various geographical latitudes.

	Total Effects		**Direct Effects**		**Indirect Effects**	
Deforestation in 70–80° N	−0.04108	(0.000)	−0.00307	(0.000)	−0.03801	(0.000)
Deforestation in 60–70° N	−0.00308	(0.100)	−0.00021	(0.143)	−0.00288	(0.097)
Deforestation in 50–60° N	−0.00709	(0.071)	−0.00045	(0.112)	−0.00665	(0.070)
Deforestation in 40–50° N	−0.00766	(0.092)	−0.00054	(0.129)	−0.00712	(0.090)
Deforestation in 30–40° N	−0.00223	(0.406)	−0.00021	(0.325)	−0.00202	(0.415)
Deforestation in 20–30° N	0.03506	(0.000)	0.00286	(0.000)	0.03220	(0.000)
Deforestation in 10–20° N	0.00845	(0.084)	0.00064	(0.089)	0.00780	(0.084)
Deforestation in 0–10° N	−0.01698	(0.000)	−0.00127	(0.000)	−0.01572	(0.000)
Deforestation in 0–10° S	−0.00573	(0.000)	−0.00043	(0.000)	−0.00531	(0.000)
Deforestation in 10–20° S	0.00189	(0.078)	0.00026	(0.006)	0.00163	(0.099)
Deforestation in 20–30° S	0.00432	(0.083)	0.00038	(0.060)	0.00395	(0.086)
Deforestation in 30–40° S	0.00797	(0.368)	0.00089	(0.241)	0.00708	(0.386)
Deforestation in 40–50° S	0.00433	(0.923)	0.00146	(0.714)	0.00287	(0.944)
Deforestation in 50–60° S	0.02774	(0.608)	0.00226	(0.666)	0.02549	(0.603)

The estimation results of coefficients in Table 5 are visually represented in Figure 6. The analysis of the figure reveals a pronounced symmetrical pattern centered around 10 degrees north latitude. The negligible impact of the deforestation coefficient from 30° N to 40° N reflects the presence of latitudes with neutral deforestation effects, a phenomenon supported by the theoretical literature. At higher latitudes, deforestation appears to reduce global temperatures. These observations are consistent with prior research. Deforestation similarly contributes to a rise in global temperatures in southern latitudes ranging from 10 to 30 degrees, aligning with theoretical predictions. However, within the equatorial belt of 10° N to 10° S, encompassing the Amazon, Congo Basin, and Southeast Asian Rainforests, deforestation surprisingly results in a decrease in global temperature, challenging the theoretical expectations—the separate deforestation impact of these three rainforests on temperature and whether this effect is asymmetric remains unclear. Given the relatively similar environmental conditions across these forests, it seems implausible to suggest that while one or two may exert a positive influence on the temperature, the negative impact from the third could offset these benefits, resulting in an overall negative effect. Therefore, the impacts in certain forests, if not outrightly negative, might be neutral or marginally positive. Our findings, hence, question deforestation's widely recognized positive impacts on the temperature at this latitude, as posited in theoretical discussions. This discrepancy suggests that the standard theoretical models based on specific assumptions and constraints may overlook particular dynamics. Consequently, our empirical findings indicate that these models have overestimated the cooling effects of forests in the 10° N to 10° S latitude band.

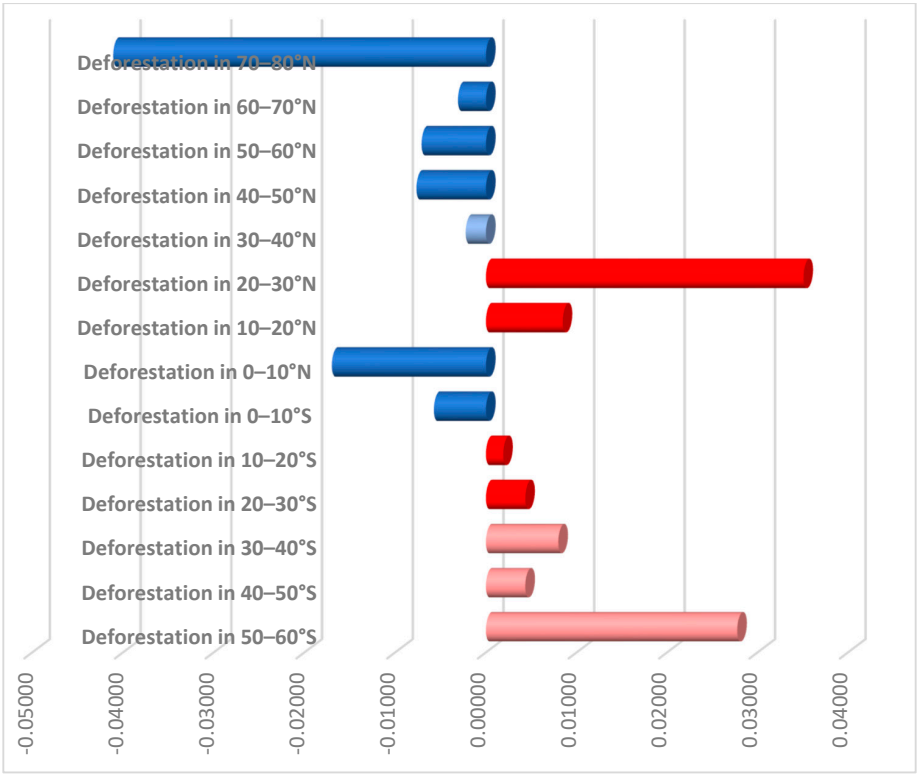

Figure 6. The marginal effects of total deforestation across various geographical latitudes. Analyzing the data presented in Table 5, it is evident that deforestation's impact on temperature variations is not significant across some latitudes designated in shades of pale blue and red. Meanwhile, the results illustrate minimal deforestation activity between latitudes 30° S and 60° S. This restricted range of observations could potentially elevate the variance of the estimated coefficients, rendering them insignificant. Conversely, the latitude range of 30° N to 40° N does not exhibit these limitations, and its meaningless coefficient should be the natural result of the lack of effect of deforestation on global temperature.

In Table 6, we delve into a more detailed examination, assessing the consequences of deforestation and the conversion of forested land to various non-forest land types, again across different geographical longitudes, estimating 56 models. To achieve our objective, we conducted estimations for 14 models across various latitudes, focusing on four distinct types of non-forest cover. We must highlight that we report only the significant effects observed at each latitude. Analyzing the data from latitudes between 10 degrees south and 10 degrees north reveals that transforming forests into croplands, grass/shrublands, and areas with sparse or no vegetation significantly reduces temperatures. Notably, the shift from forest to sparse or no vegetation, enhancing the albedo effect, results in a more pronounced temperature drop. However, Figure 7 indicates that such transformations to sparse vegetation are minimal within this specific latitude range. Moreover, while forest-to-pasture conversions are the second most common, their impact on temperature variation is not markedly significant.

Table 6. Marginal effects of deforestation and the conversion of forested land to various non-forest land types.

	Type	**Coefficient**	***p*-Value**
30–40° S	Deforestation (Forest to Pasture) in 30–40° S	0.01844	(0.044)
20–30° S	Deforestation (Forest to Grass/shrubland) in 20–30° S	0.05693	(0.014)
	Deforestation (Forest to Pasture) in 20–30° S	0.00650	(0.052)
10–20° S	Deforestation (Forest to Cropland) in 10–20° S	0.01849	(0.048)
	Deforestation (Forest to Grass/shrubland) in 10–20° S	0.02754	(0.001)
	Deforestation (Forest to Pasture) in 10–20° S	0.00275	(0.049)
	Deforestation (Forest to Sparse/ no vegetation) in 10–20° S	−0.33044	(0.047)
0–10° S	Deforestation (Forest to Cropland) in 0–10° S	−0.04226	(0.000)
	Deforestation (Forest to Grass/shrubland) in 0–10° S	−0.00762	(0.000)
	Deforestation (Forest to Sparse/ no vegetation) in 0–10° S	−0.31926	(0.000)
0–10° N	Deforestation (Forest to Cropland) in 0–10° N	−0.04826	(0.000)
	Deforestation (Forest to Grass/shrubland) in 0–10° N	−0.02919	(0.000)
	Deforestation (Forest to Sparse/ no vegetation) in 0–10° N	−0.55969	(0.000)
10–20° N	Deforestation (Forest to Grass/shrubland) in 10–20° N	0.02738	(0.009)
20–30° N	Deforestation (Forest to Cropland) in 20–30° N	0.04372	(0.000)
	Deforestation (Forest to Pasture) in 20–30° N	0.06227	(0.000)
	Deforestation (Forest to Sparse/ no vegetation) in 20–30° N	0.07658	(0.040)
60–70° N	Deforestation (Forest to Cropland) in 60–70° N	0.31744	(0.057)
	Deforestation (Forest to Grass/shrubland) in 60–70° N	−0.00458	(0.013)
	Deforestation (Forest to Pasture) in 60–70° N	0.02348	(0.004)
	Deforestation (Forest to Sparse/ no vegetation) in 60–70° N	−0.23547	(0.010)
70–80° N	Deforestation (Forest to Grass/shrubland) in 70–80° N	−0.04124	(0.000)

Contrary to other deforested lands, the greenhouse gas emissions from livestock in pastures mitigate the initial adverse effects on the temperature, a trend observed across various latitudes. Consequently, Forest conversions to Pasture generally have neutral or positive impacts on global temperatures, contradicting their perceived role in exacerbating global warming. The influence of land-use changes on temperature varies by latitude and the type of land conversion, offering valuable insights for policymakers and researchers regarding the environmental impacts of land use.

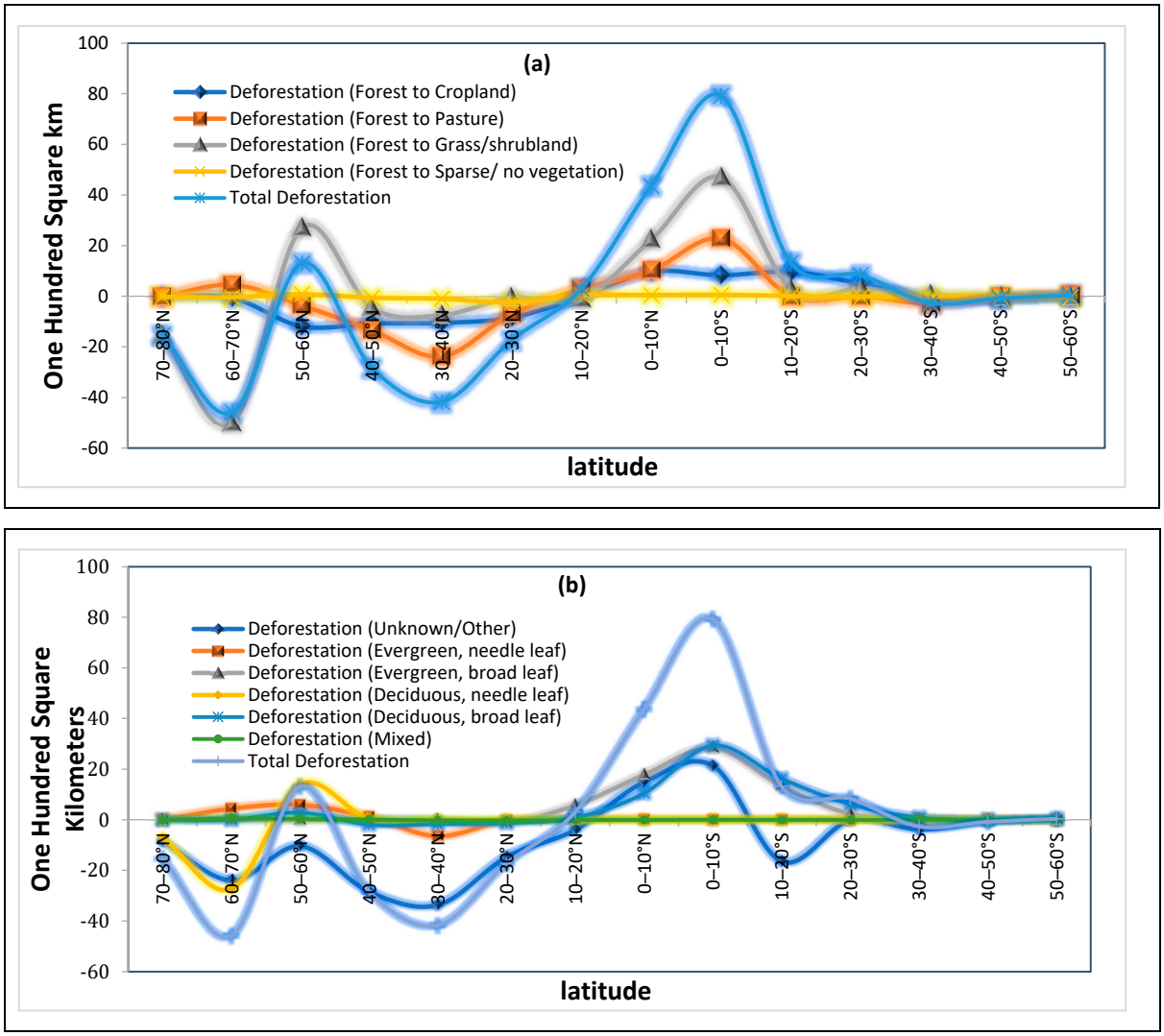

Figure 7. (**a**) **Cumulative deforestation from 1970 to 2019 across various geographical longitudes.** (**b**) **Cumulative deforestation from 1970 to 2019 for different forest types across various geographical longitudes.** Afforestation efforts have been observed at the northern latitudes, contrasting sharply with significant deforestation activities at the lower latitudes. The extent of deforestation reaches its zenith at latitudes between 10 degrees south and 10 degrees north.

4. Discussion

It is crucial to note that our results do not contradict those obtained from field measurements but complement them. While the present study does not delve into this issue in detail, we can illustratively look at recent research on the Amazon forest as an example of the work in this area. The research conducted by Pangala et al. [46] reveals that methane (CH4) emissions in the Amazon, primarily released through trees in wetlands, significantly exceed previous estimates, marking them as a significant contributor to regional and global methane emissions, 200 times greater than those observed in temperate wet forests [65] and tropical peat swamp forests [66]. This process results in remarkably higher methane outputs from Amazonian trees than those from temperate and tropical forests, highlighting the Amazon as a crucial source of non-ebullition wetland methane fluxes. Further studies by Covey et al. [47] corroborate these findings, indicating that the Amazon's methane emissions are a critical factor in global emissions, with a notable share coming from natural wetlands. The underestimation of tree-mediated methane emissions underscores a gap in our understanding of the Amazon's biogeochemical impact, particularly in global cli-

mate dynamics. In an extensive study conducted by Gatti et al. [45] involving 590 vertical profiling measurements of carbon dioxide and carbon monoxide concentrations across Amazonia from 2010 to 2018, significant insights were revealed regarding the region's carbon dynamics. The research indicates that factors such as an intensified dry season and increased deforestation rates have led to heightened ecosystem stress, frequent fires, and elevated carbon emissions, particularly in the eastern Amazon. Notably, the study uncovered that even in western Amazonian forests, where the deforestation rates are as low as 7%, more carbon is released than absorbed. These findings challenge previously held theories about the Amazon's capacity for carbon sequestration, suggesting that its ability to act as a carbon sink may have been overestimated. However, future research could benefit from a comprehensive analysis and comparison between the findings of this study and those derived from field observations in the Amazon forests and other global regions.

5. Conclusions

The thermal dynamics engendered by deforestation are governed by a nuanced equilibrium of antagonistic effects: on the one hand, warming arises from augmented atmospheric CO_2 levels and diminished latent heat flux; on the other hand, cooling results from an increased albedo. Consequently, these intricate consequences of deforestation pose a formidable challenge to the theoretical models attempting to capture its impacts on climate change. This research introduces a groundbreaking empirical model that integrates spatial panel models with satellite imagery data from 1970 to 2019, intending to reconcile the gap between theoretical climate impact predictions and empirical observations. This study stands at the forefront of innovation by quantitatively assessing the regional temperature fluctuations, examining the effects of greenhouse gas emissions, deforestation, and various meteorological and global factors, such as sunspot activity, the Earth's rotation period, and the Global Mean Sea Level. By providing new insights, this work marks a significant advancement in environmental analysis.

Furthermore, the theoretical frameworks undergirding these models have progressively embraced complexity. This trend is particularly pronounced in the analyses of the influence of forest biophysics on climate, which demonstrates significant spatial heterogeneity. However, these effects exhibit discernible patterns across various latitudinal zones despite this variability.

The findings indicate that deforestation significantly contributes to increased global temperatures across the southern latitudes, spanning 10 to 30 degrees, consistent with the theoretical forecasts. Conversely, in the equatorial zone stretching from 10° N to 10° S—an area that includes the Amazon, Congo Basin, and Southeast Asian Rainforests—deforestation unexpectedly leads to a reduction in global temperatures, thereby defying the theoretical predictions. The discrepancy highlights the necessity for further research to investigate the underlying reasons. In this work, we have equipped researchers with an empirical-based tool to guide the exploration of global phenomena. Essentially, we have charted a course for future research endeavors.

Funding: This research received no external funding.

Institutional Review Board Statement: Not applicable.

Informed Consent Statement: Not applicable.

Data Availability Statement: Software and data are available at: https://github.com/mohsenkhezrieco/Khezri.git (accessed on 17 June 2024).

Conflicts of Interest: The authors declare that they have no known competing financial interests or personal relationships that could have appeared to influence the work reported in this paper.

References

1. Bonan, G.B. Forests and Climate Change: Forcings, Feedbacks, and the Climate Benefits of Forests. *Science* **2008**, *320*, 1444–1449. [CrossRef] [PubMed]
2. Hansen, M.C.; Potapov, P.V.; Moore, R.; Hancher, M.; Turubanova, S.A.; Tyukavina, A.; Thau, D.; Stehman, S.V.; Goetz, S.J.; Loveland, T.R.; et al. High-Resolution Global Maps of 21st-Century Forest Cover Change. *Science* **2013**, *342*, 850–853. [CrossRef] [PubMed]
3. Hamers, E.M.; Maier, H.R.; Zecchin, A.C.; van Delden, H. Framework for Considering the Interactions between Climate Change, Socio-Economic Development and Land Use Planning in the Assessment of Future Flood Risk. *Environ. Model. Softw.* **2024**, *171*, 105886. [CrossRef]
4. Vilar, L.; Herrera, S.; Tafur-García, E.; Yebra, M.; Martínez-Vega, J.; Echavarría, P.; Martín, M.P. Modelling Wildfire Occurrence at Regional Scale from Land Use/Cover and Climate Change Scenarios. *Environ. Model. Softw.* **2021**, *145*, 105200. [CrossRef]
5. Griscom, B.W.; Adams, J.; Ellis, P.W.; Houghton, R.A.; Lomax, G.; Miteva, D.A.; Schlesinger, W.H.; Shoch, D.; Siikamäki, J.V.; Smith, P.; et al. Natural Climate Solutions. *Proc. Natl. Acad. Sci. USA* **2017**, *114*, 11645–11650. [CrossRef]
6. Roe, S.; Streck, C.; Obersteiner, M.; Frank, S.; Griscom, B.; Drouet, L.; Fricko, O.; Gusti, M.; Harris, N.; Hasegawa, T.; et al. Contribution of the Land Sector to a 1.5 °C World. *Nat. Clim. Change* **2019**, *9*, 817–828. [CrossRef]
7. Luyssaert, S.; Marie, G.; Valade, A.; Chen, Y.Y.; Njakou Djomo, S.; Ryder, J.; Otto, J.; Naudts, K.; Lansø, A.S.; Ghattas, J.; et al. Trade-Offs in Using European Forests to Meet Climate Objectives. *Nature* **2018**, *562*, 259–262. [CrossRef]
8. Windisch, M.G.; Davin, E.L.; Seneviratne, S.I. Prioritizing Forestation Based on Biogeochemical and Local Biogeophysical Impacts. *Nat. Clim. Change* **2021**, *11*, 867–871. [CrossRef]
9. Friedlingstein, P.; Joel, G.; Field, C.B.; Fung, I.Y. Toward an Allocation Scheme for Global Terrestrial Carbon Models. *Glob. Change Biol.* **1999**, *5*, 755–770. [CrossRef]
10. Betts, R.A. Offset of the Potential Carbon Sink from Boreal Forestation by Decreases in Surface Albedo. *Nature* **2000**, *408*, 187–190. [CrossRef]
11. Bala, G.; Caldeira, K.; Wickett, M.; Phillips, T.J.; Lobell, D.B.; Delire, C.; Mirin, A. Combined Climate and Carbon-Cycle Effects of Large-Scale Deforestation. *Proc. Natl. Acad. Sci. USA* **2007**, *104*, 6550–6555. [CrossRef] [PubMed]
12. Song, X.P.; Hansen, M.C.; Stehman, S.V.; Potapov, P.V.; Tyukavina, A.; Vermote, E.F.; Townshend, J.R. Global Land Change from 1982 to 2016. *Nature* **2018**, *560*, 639–643. [CrossRef] [PubMed]
13. Ge, J.; Liu, Q.; Zan, B.; Lin, Z.; Lu, S.; Qiu, B.; Guo, W. Deforestation Intensifies Daily Temperature Variability in the Northern Extratropics. *Nat. Commun.* **2022**, *13*, 5955. [CrossRef] [PubMed]
14. Bonan, G.B.; Pollard, D.; Thompson, S.L. Effects of Boreal Forest Vegetation on Global Climate. *Nature* **1992**, *359*, 716–718. [CrossRef]
15. Brovkin, V.; Ganopolski, A.; Claussen, M.; Kubatzki, C.; Petoukhov, V. Modelling Climate Response to Historical Land Cover Change. *Glob. Ecol. Biogeogr.* **1999**, *8*, 509–517. [CrossRef]
16. Bonan, G.B. Observational Evidence for Reduction of Daily Maximum Temperature by Croplands in the Midwest United States. *J. Clim.* **2001**, *14*, 2430–2442. [CrossRef]
17. Matthews, H.D.; Weaver, A.J.; Meissner, K.J.; Gillett, N.P.; Eby, M. Natural and Anthropogenic Climate Change: Incorporating Historical Land Cover Change, Vegetation Dynamics and the Global Carbon Cycle. *Clim. Dyn.* **2004**, *22*, 461–479. [CrossRef]
18. Bounoua, L.; DeFries, R.; Collatz, G.J.; Sellers, P.; Khan, H. Effects of Land Cover Conversion on Surface Climate. *Clim. Change* **2002**, *52*, 29–64. [CrossRef]
19. Davin, E.L.; de Noblet-Ducoudre, N. Climatic Impact of Global-Scale Deforestation: Radiative versus Nonradiative Processes. *J. Clim.* **2010**, *23*, 97–112. [CrossRef]
20. Mildrexler, D.J.; Zhao, M.; Running, S.W. A Global Comparison between Station Air Temperatures and MODIS Land Surface Temperatures Reveals the Cooling Role of Forests. *J. Geophys. Res. Biogeosci.* **2011**, *116*, G03025. [CrossRef]
21. Alkama, R.; Cescatti, A. Climate Change: Biophysical Climate Impacts of Recent Changes in Global Forest Cover. *Science* **2016**, *351*, 600–604. [CrossRef]
22. Kleidon, A.; Fraedrich, K.; Heimann, M. A Green Planet versus a Desert World: Estimating the Maximum Effect of Vegetation on the Land Surface Climate. *Clim. Change* **2000**, *44*, 471–493. [CrossRef]
23. Govindasamy, B.; Duffy, P.B.; Caldeira, K. Land Use Changes and Northern Hemisphere Cooling. *Geophys. Res. Lett.* **2001**, *28*, 291–294. [CrossRef]
24. Findell, K.L.; Shevliakova, E.; Milly, P.C.D.; Stouffer, R.J. Modeled Impact of Anthropogenic Land Cover Change on Climate. *J. Clim.* **2007**, *20*, 3621–3634. [CrossRef]
25. Bright, R.M.; Zhao, K.; Jackson, R.B.; Cherubini, F. Quantifying Surface Albedo and Other Direct Biogeophysical Climate Forcings of Forestry Activities. *Glob. Change Biol.* **2015**, *21*, 3246–3266. [CrossRef]
26. Perugini, L.; Caporaso, L.; Marconi, S.; Cescatti, A.; Quesada, B.; De Noblet-Ducoudré, N.; House, J.I.; Arneth, A. Biophysical Effects on Temperature and Precipitation Due to Land Cover Change. *Environ. Res. Lett.* **2017**, *12*, 053002. [CrossRef]

27. Lee, S.H.; Yamakawa, Y.; Peng, M.W.; Barney, J.B. How Do Bankruptcy Laws Affect Entrepreneurship Development around the World? *J. Bus. Ventur.* **2011**, *26*, 505–520. [CrossRef]
28. Findell, K.L.; Berg, A.; Gentine, P.; Krasting, J.P.; Lintner, B.R.; Malyshev, S.; Santanello, J.A.; Shevliakova, E. The Impact of Anthropogenic Land Use and Land Cover Change on Regional Climate Extremes. *Nat. Commun.* **2017**, *8*, 989. [CrossRef]
29. Lejeune, Q.; Davin, E.L.; Gudmundsson, L.; Winckler, J.; Seneviratne, S.I. Historical Deforestation Locally Increased the Intensity of Hot Days in Northern Mid-Latitudes. *Nat. Clim. Change* **2018**, *8*, 386–390. [CrossRef]
30. Bathiany, S.; Claussen, M.; Brovkin, V.; Raddatz, T.; Gayler, V. Combined Biogeophysical and Biogeochemical Effects of Large-Scale Forest Cover Changes in the MPI Earth System Model. *Biogeosciences* **2010**, *7*, 1383–1399. [CrossRef]
31. Claussen, M.; Brovkin, V.; Ganopolski, A. Biophysical versus Biogeochemical Feedbacks of Large-Scale Land Cover Change. *Geophys. Res. Lett.* **2001**, *28*, 1011–1014. [CrossRef]
32. de Oliveira Serrão, E.A.; Silva, M.T.; Ferreira, T.R.; Freitas Xavier, A.C.; dos Santos, C.A.; Paiva de Ataide, L.C.; Pontes, P.R.M.; Rodrigues da Silva, V. de P. Climate and Land Use Change: Future Impacts on Hydropower and Revenue for the Amazon. *J. Clean. Prod.* **2023**, *385*, 135700. [CrossRef]
33. Li, Y.; Zhao, M.; Motesharrei, S.; Mu, Q.; Kalnay, E.; Li, S. Local Cooling and Warming Effects of Forests Based on Satellite Observations. *Nat. Commun.* **2015**, *6*, 6603. [CrossRef] [PubMed]
34. Anderson, R.G.; Canadell, J.G.; Randerson, J.T.; Jackson, R.B.; Hungate, B.A.; Baldocchi, D.D.; Ban-Weiss, G.A.; Bonan, G.B.; Caldeira, K.; Cao, L.; et al. Biophysical Considerations in Forestry for Climate Protection. *Front. Ecol. Environ.* **2011**, *9*, 174–182. [CrossRef]
35. Zhang, H.; Henderson-Sellers, A.; Mcguffie, K. The Compounding Effects of Tropical Deforestation and Greenhouse Warming on Climate. *Clim. Change* **2001**, *49*, 309–338. [CrossRef]
36. Lee, X.; Goulden, M.L.; Hollinger, D.Y.; Barr, A.; Black, T.A.; Bohrer, G.; Bracho, R.; Drake, B.; Goldstein, A.; Gu, L.; et al. Observed Increase in Local Cooling Effect of Deforestation at Higher Latitudes. *Nature* **2011**, *479*, 384–387. [CrossRef]
37. Pitman, A.J.; De Noblet-Ducoudré, N.; Cruz, F.T.; Davin, E.L.; Bonan, G.B.; Brovkin, V.; Claussen, M.; Delire, C.; Ganzeveld, L.; Gayler, V.; et al. Uncertainties in Climate Responses to Past Land Cover Change: First Results from the LUCID Intercomparison Study. *Geophys. Res. Lett.* **2009**, *36*, L14814. [CrossRef]
38. De Noblet-Ducoudré, N.; Boisier, J.P.; Pitman, A.; Bonan, G.B.; Brovkin, V.; Cruz, F.; Delire, C.; Gayler, V.; Van Den Hurk, B.J.J.M.; Lawrence, P.J.; et al. Determining Robust Impacts of Land-Use-Induced Land Cover Changes on Surface Climate over North America and Eurasia: Results from the First Set of LUCID Experiments. *J. Clim.* **2012**, *25*, 3261–3281. [CrossRef]
39. Bright, R.M.; Davin, E.; O'Halloran, T.; Pongratz, J.; Zhao, K.; Cescatti, A. Local Temperature Response to Land Cover and Management Change Driven by Nonradiative Processes. *Nat. Clim. Change* **2017**, *7*, 296–302. [CrossRef]
40. Schultz, N.M.; Lawrence, P.J.; Lee, X. Global Satellite Data Highlights the Diurnal Asymmetry of the Surface Temperature Response to Deforestation. *J. Geophys. Res. Biogeosci.* **2017**, *122*, 903–917. [CrossRef]
41. Taylor, K.E.; Stouffer, R.J.; Meehl, G.A. An Overview of CMIP5 and the Experiment Design. *Bull. Am. Meteorol. Soc.* **2012**, *93*, 485–498. [CrossRef]
42. Chen, L.; Dirmeyer, P.A. Reconciling the Disagreement between Observed and Simulated Temperature Responses to Deforestation. *Nat. Commun.* **2020**, *11*, 202. [CrossRef] [PubMed]
43. Li, X.; Chen, H.; Wei, J.; Hua, W.; Sun, S.; Ma, H.; Li, X.; Li, J. Inconsistent Responses of Hot Extremes to Historical Land Use and Cover Change Among the Selected CMIP5 Models. *J. Geophys. Res. Atmos.* **2018**, *123*, 3497–3512. [CrossRef]
44. Lejeune, Q.; Seneviratne, S.I.; Davin, E.L. Historical Land-Cover Change Impacts on Climate: Comparative Assessment of LUCID and CMIP5 Multimodel Experiments. *J. Clim.* **2017**, *30*, 1439–1459. [CrossRef]
45. Gatti, L.V.; Basso, L.S.; Miller, J.B.; Gloor, M.; Gatti Domingues, L.; Cassol, H.L.G.; Tejada, G.; Aragão, L.E.O.C.; Nobre, C.; Peters, W.; et al. Amazonia as a Carbon Source Linked to Deforestation and Climate Change. *Nature* **2021**, *595*, 388–393. [CrossRef]
46. Pangala, S.R.; Enrich-Prast, A.; Basso, L.S.; Peixoto, R.B.; Bastviken, D.; Hornibrook, E.R.C.; Gatti, L.V.; Marotta, H.; Calazans, L.S.B.; Sakuragui, C.M.; et al. Large Emissions from Floodplain Trees Close the Amazon Methane Budget. *Nature* **2017**, *552*, 230–234. [CrossRef]
47. Covey, K.; Soper, F.; Pangala, S.; Bernardino, A.; Pagliaro, Z.; Basso, L.; Cassol, H.; Fearnside, P.; Navarrete, D.; Novoa, S.; et al. Carbon and Beyond: The Biogeochemistry of Climate in a Rapidly Changing Amazon. *Front. For. Glob. Change* **2021**, *4*, 618401. [CrossRef]
48. Stern, D.I.; Kaufmann, R.K. Econometric Analysis of Global Climate Change. *Environ. Model. Softw.* **1999**, *14*, 597–605. [CrossRef]
49. Liu, H.; Rodríguez, G. Human Activities and Global Warming: A Cointegration Analysis. *Environ. Model. Softw.* **2005**, *20*, 761–773. [CrossRef]
50. Pretis, F. Econometric Modelling of Climate Systems: The Equivalence of Energy Balance Models and Cointegrated Vector Autoregressions. *J. Econom.* **2020**, *214*, 256–273. [CrossRef]
51. Newell, R.G.; Prest, B.C.; Sexton, S.E. The GDP-Temperature Relationship: Implications for Climate Change Damages. *J. Environ. Econ. Manag.* **2021**, *108*, 102445. [CrossRef]

52. Ma, B.; Karimi, M.S.; Mohammed, K.S.; Shahzadi, I.; Dai, J. Nexus between Climate Change, Agricultural Output, Fertilizer Use, Agriculture Soil Emissions: Novel Implications in the Context of Environmental Management. *J. Clean. Prod.* **2024**, *450*, 141801. [CrossRef]
53. Anselin, L.; Le Gallo, J.; Jayet, H. Spatial Panel Econometrics. *Adv. Stud. Theor. Appl. Econom.* **2008**, *46*, 625–660. [CrossRef]
54. LeSage, J.P.; Fischer, M.M. Spatial Growth Regressions: Model Specification, Estimation and Interpretation. *Spat. Econ. Anal.* **2008**, *3*, 275–304. [CrossRef]
55. Modiri, S.; Belda, S.; Hoseini, M.; Heinkelmann, R.; Ferrándiz, J.M.; Schuh, H. A New Hybrid Method to Improve the Ultra-Short-Term Prediction of LOD. *J. Geod.* **2020**, *94*, 23. [CrossRef]
56. Gross, R.S.; Marcus, S.L.; Eubanks, T.M.; Dickey, J.O.; Keppenne, C.L. Detection of an ENSO Signal in Seasonal Length-of-Day Variations. *Geophys. Res. Lett.* **1996**, *23*, 3373–3376. [CrossRef]
57. Zotov, L.; Bizouard, C.; Shum, C.K. A Possible Interrelation between Earth Rotation and Climatic Variability at Decadal Time-Scale. *Geod. Geodyn.* **2016**, *7*, 216–222. [CrossRef]
58. Ding, H.; Jin, T.Y.; Li, J.C.; Jiang, W.P. The Contribution of a Newly Unraveled 64 Years Common Oscillation on the Estimate of Present-Day Global Mean Sea Level Rise. *J. Geophys. Res. Solid Earth* **2021**, *126*, e2021JB022147. [CrossRef]
59. Winkler, K.; Fuchs, R.; Rounsevell, M.D.A.; Herold, M. HILDA+ Global Land Use Change between 1960 and 2019. 2020. Available online: https://doi.pangaea.de/10.1594/PANGAEA.921846 (accessed on 21 January 2024).
60. Crippa, M.; Guizzardi, D.; Schaaf, E.; Monforti-Ferrario, F.; Quadrelli, R.; Risquez Martin, A.; Rossi, S.; Vignati, E.; Muntean, M.; Brandao De Melo, J.; et al. *GHG Emissions of All World Countries—2023*; Publications Office of the European Union: Luxembourg, 2023.
61. Hersbach, H.; Bell, B.; Berrisford, P.; Biavati, G.; Horányi, A.; Muñoz Sabater, J.; Nicolas, J.; Peubey, C.; Radu, R.; Rozum, I.; et al. ERA5 Hourly Data on Single Levels from 1940 to Present. *Copernicus Clim. Change Serv. Clim. Data Store* **2023**, *147*, 4186–4227.
62. Frederikse, T.; Landerer, F.; Caron, L.; Adhikari, S.; Parkes, D.; Humphrey, V.W.; Dangendorf, S.; Hogarth, P.; Zanna, L.; Cheng, L.; et al. The Causes of Sea-Level Rise since 1900. *Nature* **2020**, *584*, 393–397. [CrossRef]
63. Beckley, B.; Ray, R.; Zelensky, N.; Lemoine, F.; Yang, X.; Brown, S.; Desai, S.; Mitchum, G. Global Mean Sea Level Trend from Integrated Multi-Mission Ocean Altimeters TOPEX/Poseidon, Jason-1, OSTM/Jason-2, and Jason-3 Version 5.1. Ver. 5.1. PO.DAAC, CA, USA. [CrossRef]
64. Bjørnstad, O.N.; Falck, W. Nonparametric Spatial Covariance Functions: Estimation and Testing. *Environ. Ecol. Stat.* **2001**, *8*, 53–70. [CrossRef]
65. Pangala, S.R.; Hornibrook, E.R.C.; Gowing, D.J.; Gauci, V. The Contribution of Trees to Ecosystem Methane Emissions in a Temperate Forested Wetland. *Glob. Change Biol.* **2015**, *21*, 2642–2654. [CrossRef] [PubMed]
66. Pangala, S.R.; Moore, S.; Hornibrook, E.R.C.; Gauci, V. Trees Are Major Conduits for Methane Egress from Tropical Forested Wetlands. *New Phytol.* **2013**, *197*, 524–531. [CrossRef] [PubMed]